Science
AAAS

Visualizing Antigen-Specific and Infected Cells in Situ Predicts Outcomes in Early Viral Infection
Qingsheng Li, *et al.*
Science **323**, 1726 (2009);
DOI: 10.1126/science.1168676

The following resources related to this article are available online at www.sciencemag.org (this information is current as of March 27, 2009):

Updated information and services, including high-resolution figures, can be found in the online version of this article at:
http://www.sciencemag.org/cgi/content/full/323/5922/1726

Supporting Online Material can be found at:
http://www.sciencemag.org/cgi/content/full/323/5922/1726/DC1

This article **cites 19 articles**, 14 of which can be accessed for free:
http://www.sciencemag.org/cgi/content/full/323/5922/1726#otherarticles

This article appears in the following **subject collections**:
Virology
http://www.sciencemag.org/cgi/collection/virology

Information about obtaining **reprints** of this article or about obtaining **permission to reproduce this article** in whole or in part can be found at:
http://www.sciencemag.org/about/permissions.dtl

Downloaded from www.sciencemag.org on March 27, 2009

Science (print ISSN 0036-8075; online ISSN 1095-9203) is published weekly, except the last week in December, by the American Association for the Advancement of Science, 1200 New York Avenue NW, Washington, DC 20005. Copyright 2009 by the American Association for the Advancement of Science; all rights reserved. The title *Science* is a registered trademark of AAAS.

Visualizing Antigen-Specific and Infected Cells in Situ Predicts Outcomes in Early Viral Infection

Qingsheng Li,[1] Pamela J. Skinner,[2] Sang-Jun Ha,[3] Lijie Duan,[1] Teresa L. Mattila,[2] Aaron Hage,[2] Cara White,[2] Daniel L. Barber,[4] Leigh O'Mara,[3] Peter J. Southern,[1] Cavan S. Reilly,[5] John V. Carlis,[6] Christopher J. Miller,[7] Rafi Ahmed,[3] Ashley T. Haase[1]*

In the early stages of viral infection, outcomes depend on a race between expansion of infection and the immune response generated to contain it. We combined in situ tetramer staining with in situ hybridization to visualize, map, and quantify relationships between immune effector cells and their targets in tissues. In simian immunodeficiency virus infections in macaques and lymphocytic choriomeningitis virus infections in mice, the magnitude and timing of the establishment of an excess of effector cells versus targets were found to correlate with the extent of control and the infection outcome (i.e., control and clearance versus partial or poor control and persistent infection). This method highlights the importance of the location, timing, and magnitude of the immune response needed for a vaccine to be effective against agents of persistent infection, such as HIV-1.

The outcome of viral infections in the acute stage of infection can be thought of as a numbers game and race, with the magnitude and speed of mounting host defenses competing against virus propagation and spread (*1*). Generally, in self-limited and fully controlled infections, the host wins by quickly generating large numbers of virus-specific cytotoxic T lymphocytes (CTLs) that terminate infection by clearing infected cells. However, a virus can win, and can establish a persistent infection, when the cellular immune response is delayed and is of insufficient magnitude to clear infection. The outcome then depends on the extent to which the CTL response can control infection and prevent progression to disease.

We studied correlates of these different outcomes of infection in simian immunodeficiency virus (SIV) and lymphocytic choriomeningitis virus (LCMV) infections. SIV (and HIV-1) cause persistent infections in which the CTL response in the early stages of infection (*2*, *3*) is too little and too late (*4*–*7*) to prevent systemic infection and massive depletion of $CD4^+$ T cells in the gut (*8*–*10*), but is usually sufficient to partially control virus production (*2*, *3*). LCMV strains cause infections in which the outcome may be clearance or persistence, depending on the strain: Infection with LCMV-Armstrong is cleared from adult C57B1/6 mice by 8 days post-inoculation (dpi), whereas animals infected with LCMV–clone 13 remain persistently viremic for months (*11*, *12*).

To identify correlates of clearance and the extent of control in persistent infections, we investigated the relationship between increasing numbers of infected cells and virus-specific CTLs in the early stages of SIV and LCMV infections. We hypothesized that the outcomes of infection would be determined by the timing, ratio, and spatial colocalization of virus-specific CTLs to infected cells. We tested this hypothesis with a method (*13*) called ISTH, as it combines in situ tetramer (IST) staining (*14*) and in situ hybridization (ISH) to locate and enumerate virus-specific $tetramer^+$ T cells and viral RNA^+ cells in tissues, using these as measures, respectively, of virus-specific CTLs and infected cells.

After intravaginal inoculation of SIV into adult female rhesus macaques, virus replicates in the first week in cervical vaginal tissues and then spreads throughout the lymphatic tissues to reach a peak in numbers of infected cells at 10 to 14 dpi (*8*, *15*). The peak in viral replication precedes the cellular immune response to immunodominant epitopes in SIV Gag and Tat that together constitute 70% of the cellular immune response in acute infection (*16*). This response is not detected until 14 dpi (*7*), which is too late to prevent a robust systemic infection. However, numbers of SIV RNA^+ cells do decline between 14 and 28 dpi, at a time coinciding with the detection of increasing numbers of Gag- and Tat-$tetramer^+$ cells by fluorescence-activated cell sorting (FACS) analysis and IST staining (*7*).

This decline in SIV RNA^+ cells was greater in cervical vaginal tissues than in lymphatic tissues (*15*), consistent with the hypothesis that the extent of control in each tissue compartment was related to the spatial proximity and numbers of $tetramer^+$ cells relative to the numbers of SIV RNA^+ cells. We used ISTH to test this hypothesis by visualizing, in the same section, effector (E) $tetramer^+$ cells and target (T) SIV RNA^+ cells, and then determining E:T cell ratios and the spatial proximity of $tetramer^+$ cells to their targets in cervical vaginal and lymphatic tissues (*13*).

We indeed found that the decline in numbers of infected cells in the cervix between the peak and 21 dpi (fig. S1, A and B) was correlated with detection by ISTH (Fig. 1A) of Gag-$tetramer^+$ cell–SIV RNA^+ cell conjugates. The decline in SIV RNA^+ cells in lymphatic tissues was also correlated with increasing numbers of $tetramer^+$ cells in close proximity to infected cells, illustrated for a lymph node at 21 dpi in Fig. 1B. We captured the spatial relationships between $tetramer^+$ and SIV RNA^+ cells in this lymph node by independently plotting their positions on a two-dimensional plane (*13*). In the montage of the whole lymph node section shown in Fig. 1B, arrows in the enlarged inset from the encircled area of the montage point to a red Gag-$tetramer^+$ cell and a blue SIV RNA^+ cell. The positions of these Gag-$tetramer^+$ cells are outlined against a gray-white mask of the section in Fig. 2A, and the positions of the Gag-$tetramer^+$ cell centers (centroids) are plotted in the upper panel of Fig. 2B. The positions of SIV RNA^+ cells in this section are plotted in the middle panel of Fig. 2B. The lower panel shows, in the superimposition of the upper and middle panels, Gag-$tetramer^+$ cells and SIV RNA^+ cells in close spatial proximity to one another throughout the lymph node. We thus conclude that effectors and targets are in close spatial proximity in these two tissue compartments.

By using ISTH to determine E:T ratios, we could further show that these ratios correlated with the extent of virus control in each tissue compartment. Defining extent of control as the reduction from peak numbers of copies of SIV RNA per microgram of tissue RNA to copy numbers at 20, 21, and 28 dpi, when the animals had mounted a tetramer response and viral load data were available from previously reported studies (*15*), we found a statistically significant relationship between the E:T ratio and relative reduction ($P = 0.001$). Reductions in viral loads by a factor of 80 to 160 were correlated with E:T ratios of ≥100. These ratios, with one exception, were achieved only in the female reproductive tract tissues where initial exposure and virus replication had elicited the most robust response.

We next investigated the relationship between the timing and magnitude of the effector response to infection outcome in LCMV-Armstrong and LCMV–clone 13 infections. LCMV-Armstrong infections are rapidly cleared by the second week of infection, whereas LCMV–clone 13 infections continue at high levels for months, with debilitating effects on virus-specific CTL proliferation and function mediated by programmed cell death–1 (PD-1) and its ligands (*11*, *12*, *15*, *17*). Because the two amino acid differences between LCMV-Armstrong and LCMV–clone 13 do not alter dominant or subdominant epitopes (*18*, *19*), it is not yet clear

[1]Department of Microbiology, Medical School, University of Minnesota, Minneapolis, MN 55455, USA. [2]Department of Veterinary and Biomedical Sciences, University of Minnesota, St. Paul, MN 55108, USA. [3]Emory Vaccine Center, Department of Microbiology and Immunology, Emory University School of Medicine, Atlanta, GA 30322, USA. [4]Immunobiology Section, National Institute of Allergy and Infectious Diseases, Bethesda, MD 20892, USA. [5]Division of Biostatistics, School of Public Health, University of Minnesota, Minneapolis, MN 55455, USA. [6]Department of Computer Science and Engineering, Institute of Technology, University of Minnesota, Minneapolis, MN 55455, USA. [7]Center for Comparative Medicine, California National Primate Research Center, University of California, Davis, CA 95616, USA.

*To whom correspondence should be addressed. E-mail: haase001@umn.edu

Downloaded from www.sciencemag.org on March 27, 2009

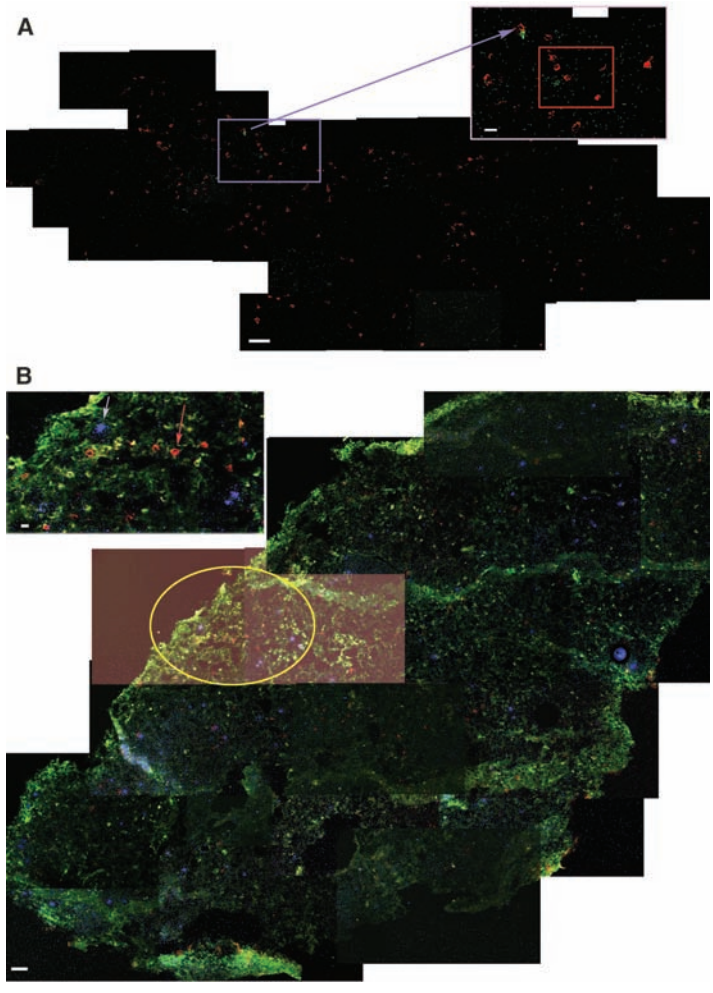

Fig. 1. ISTH analysis. (**A**) Cervical tissues, 21 dpi. The image of a whole section of cervix was reconstructed as a montage in Photoshop from separate confocal images, using the red channel for the Gag-tetramer$^+$ cells and green for the SIV RNA$^+$ cells. The blue arrow from the region enclosed by the blue rectangle points to a red Gag-tetramer$^+$ cell–green SIV RNA$^+$ cell conjugate in the enlarged inset. The excess of Gag-tetramer$^+$ cells is shown in the inset in a region enclosed by the red rectangle. (**B**) Lymphatic tissues, 21 dpi. Montage of a whole lymph node section reconstructed in Photoshop from separate images, using the red channel for the Gag-tetramer$^+$ cells, blue for the SIV RNA$^+$ cells, and green for CD8$^+$ T cells. The red arrow in the enlarged inset (upper left) points to a red Gag-tetramer$^+$ cell; the light blue arrow points to a blue SIV RNA$^+$ cell. The two lightened separate images with an encircled distinctive V-shaped constellation of Gag-tetramer$^+$ cells provide a frame of reference for Fig. 2. Scale bars for whole sections, 50 μm; insets, 10 μm.

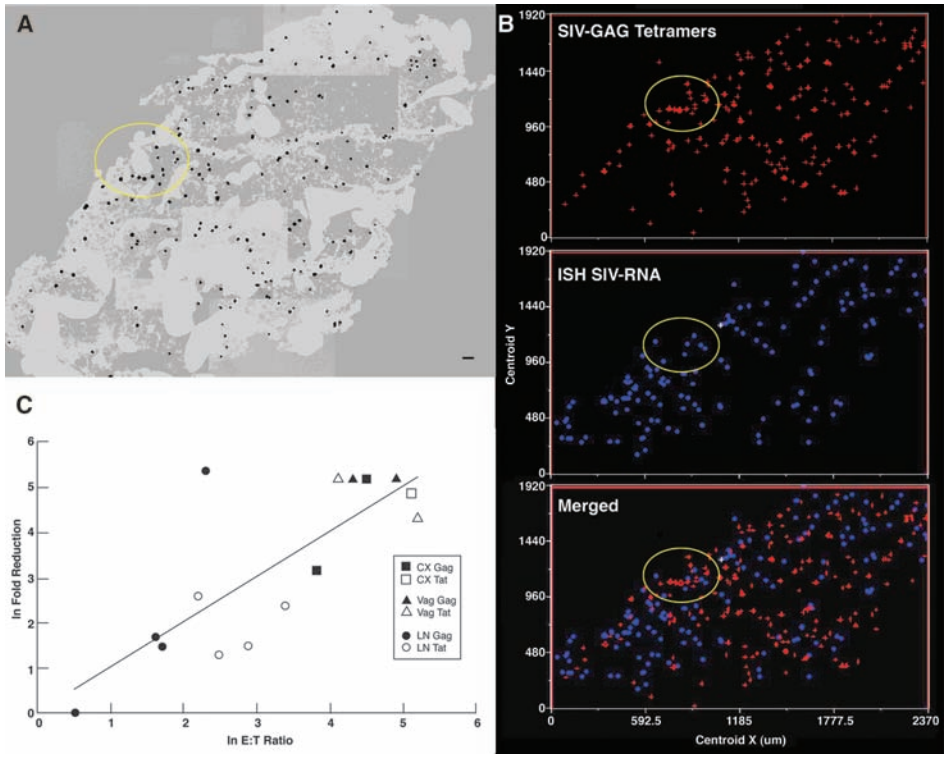

Fig. 2. Spatial relationships between SIV-tetramer$^+$ and SIV RNA$^+$ cells in the lymph node shown in Fig. 1B, and relationship between E:T ratios and reduction in viral replication. (**A**) Gag-tetramer$^+$ cells are shown against a gray-white mask of the section, with the V-shaped encircled constellation shown in Fig. 1B. Scale bar, 50 μm. (**B**) SIV RNA$^+$ and tetramer$^+$ cells were mapped by plotting the *x* and *y* coordinates of their centers (centroids) onto a two-dimensional grid measured from a fixed starting position (0,0). Upper panel, Gag-tetramer$^+$ cells; middle panel, SIV RNA$^+$ cells; lower panel, superimposition of upper and middle panels revealing the close spatial proximity of the virus-specific tetramer$^+$ cells with SIV RNA$^+$ throughout the lymph node. The white crosses and encircled areas in the panels are included as points of reference. (**C**) E:T ratio correlates with reduction in viral load in cervical vaginal and lymphatic tissues. Natural log–transformed viral load fold reductions are plotted against E:T ratios for Gag- and Tat-tetramer$^+$ cells in cervical (CX) and vaginal (Vag) tissues and lymph nodes (LN) from five animals at 20 to 28 dpi. E:T ratios were determined by ISH as described (*13*).

Downloaded from www.sciencemag.org on March 27, 2009

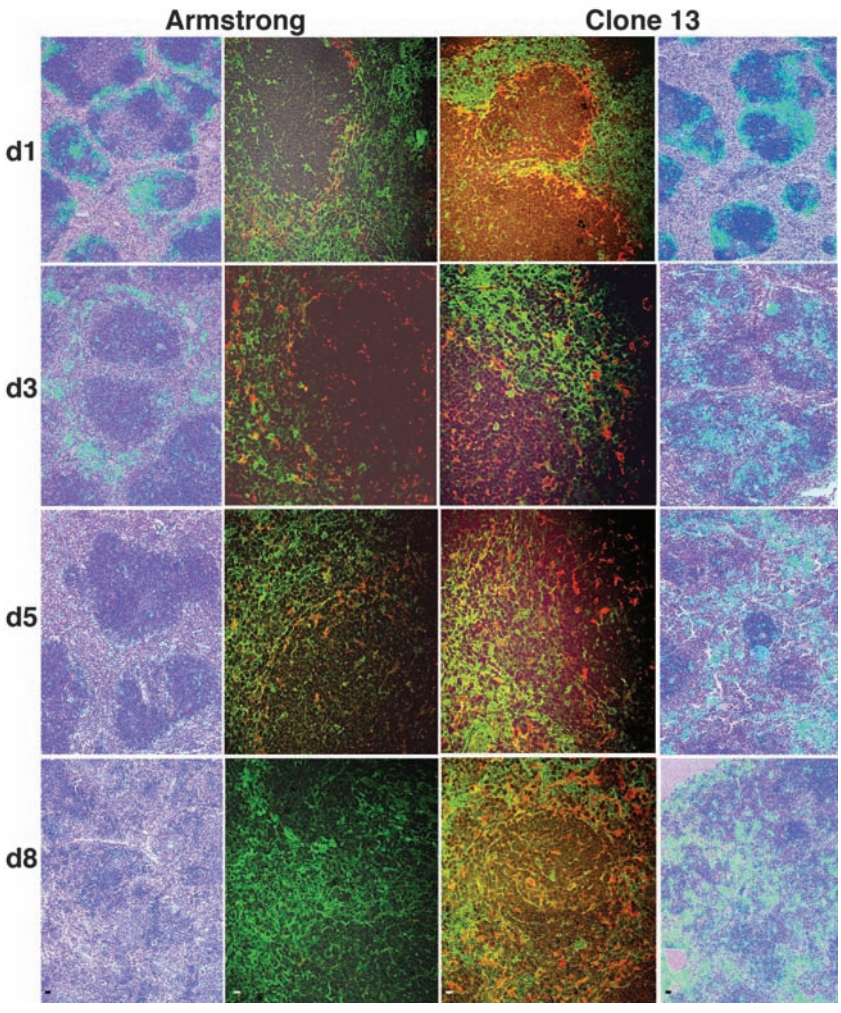

Fig. 3. Time course comparison of cells infected by LCMV-Armstrong or LCMV–clone 13. Outer columns: LCMV RNA$^+$ cells detected by ISH with LCMV-specific probes have a greenish appearance in developed radioautographs viewed in reflected light. Spleen white pulp is counterstained dark blue. Inner columns: LCMV-antigen$^+$ cells are stained red with polyclonal antibody to LCMV; FRCs in white pulp are stained green with the FRC marker ER-TR7. Both viral strains at 1 dpi (d1) infect macrophages in the marginal zone and FRCs in the white pulp, but LCMV–clone 13 infects larger numbers of both cell types. LCMV–clone 13 continues to infect large numbers of both cell types over the 8-day time course of the experiment, whereas the numbers of infected cells rapidly decline in LCMV-Armstrong infections. Scale bars (bottom row), 10 μm.

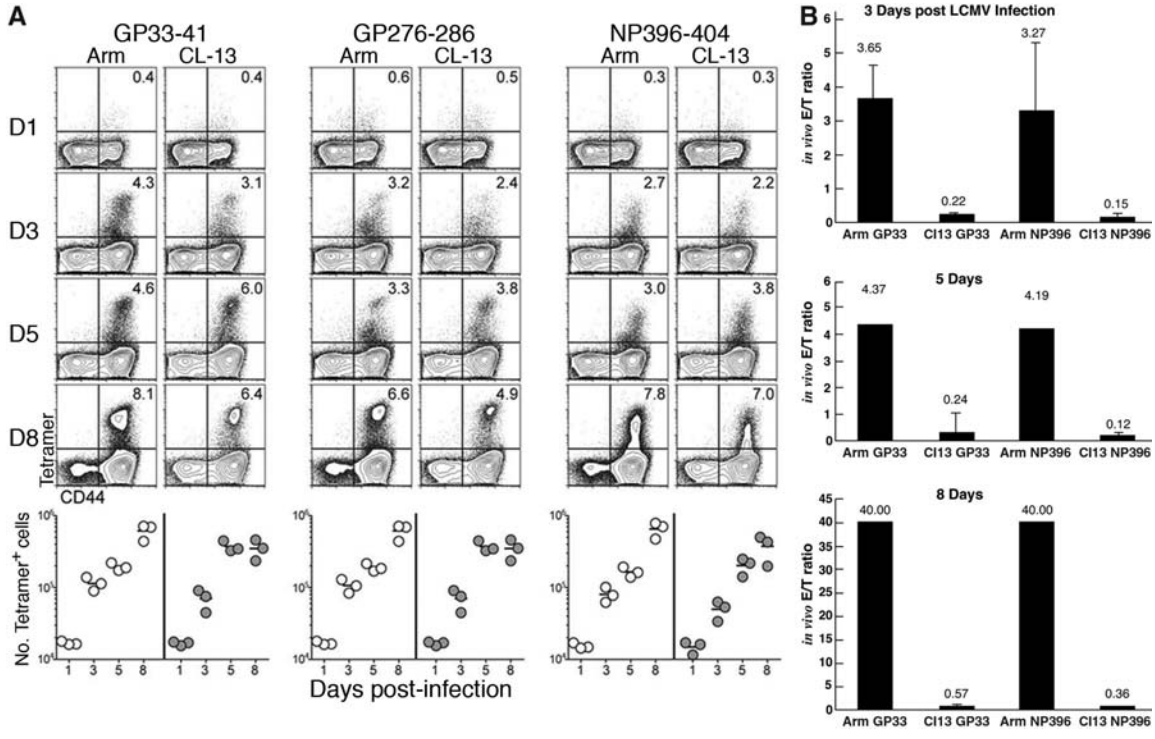

Fig. 4. (**A**) FACS analysis of the immunodominant epitope response to acute LCMV-Armstrong and LCMV–clone 13 infections in spleen. Flow cytometric quantification is presented as proportions and numbers of stained tetramer$^+$ cells from disaggregated spleens from groups of three mice per time point after LCMV-Armstrong or LCMV–clone 13 infection. Representative plots gated on CD8$^+$ T cells are shown by MHC class I tetramer (*y* axis) for each immunodominant epitope (GP33-41, GP276-286, and NP396-404) and CD44 (*x* axis). (**B**) E:T ratios in acute LCMV-Armstrong and LCMV–clone 13 infections in spleen. E:T ratios at the times shown were determined by ISTH as described (*13*).

Downloaded from www.sciencemag.org on March 27, 2009

why the initial CD8 T cell response should result in such divergent outcomes.

We determined by ISTH that strain LCMV-Armstrong is cleared because the number of immune effectors rapidly exceeds the number of infected cells. LCMV–clone 13, on the other hand, immediately infects larger numbers of macrophages (*18*) and fibroreticular cells (FRCs) (*20*) than does LCMV-Armstrong, thereby exceeding the capacity of the initial immune response to reduce the basic reproductive rate below 1 and thereby contain infection.

The divergent outcome and larger number of cells infected by LCMV–clone 13 in the spleen are illustrated in Fig. 3, which tracks LCMV RNA$^+$ cells and LCMV-antigen$^+$ FRCs (*13*) in the spleen from 1 to 8 dpi for the respective strains. As previously described, both strains of LCMV infect splenic marginal zone macrophages and FRCs in the white pulp, but LCMV–clone 13 infects larger numbers of both cell types (*18*, *20*). This difference, particularly the infection of FRCs, is already evident at 1 dpi, as judged by the diffuse ISH signal emanating from LCMV RNA$^+$ cells in the white pulp. LCMV–clone 13 infection of both cell types is sustained at high levels at 3, 5, and 8 dpi, whereas the numbers of LCMV-Armstrong–infected cells are barely detectable by 8 dpi.

The different infection outcomes produced by these two strains of LCMV cannot be explained by differences in the immune response seen in FACS analysis, but can be explained by ISTH, which provides the critical relevant measure of relative rates of increase in effectors and targets. By FACS analysis, the rapidly expanding populations of virus-specific tetramer$^+$ T cells were comparable for both strains from 3 to 8 dpi (Fig. 4A). However, E:T ratios determined by ISH reflect the increase of infected cells (relative to LCMV-GP and NP-tetramer$^+$ cells) in LCMV–clone 13 infection versus LCMV-Armstrong infection (Fig. 4B). Because of the faster increase of infected cells relative to LCMV-tetramer$^+$ cells, the E:T ratio for LCMV–clone 13 never approached 1. By contrast, the E:T ratio for LCMV-Armstrong was already ~4 at 3 dpi, higher than the ratio for LCMV–clone 13 at 3 dpi by a factor of 20.

Together, the ISTH analyses of SIV and LCMV infection tell us that location, timing, and numbers of effectors and targets all count in determining outcome. We have speculated elsewhere (*5*) that if the "too little, too late" response to SIV infection (*7*) had occurred earlier, when there were only small founder populations of infected cells confined to the portal of entry, vaginal transmission and systemic infection might be prevented with relatively few effector cells. Thus, in SIV (and, by extension, HIV-1) infections, a vaccine that elicited an immune response at the portal of entry "enough and soon enough" could prevent vaginal transmission.

References and Notes

1. P. C. Doherty, *Science* **280**, 227 (1998).
2. R. A. Koup *et al.*, *J. Virol.* **68**, 4650 (1994).
3. M. J. Kuroda *et al.*, *J. Immunol.* **162**, 5127 (1999).
4. M. P. Davenport, R. M. Ribeiro, A. S. Perelson, *J. Virol.* **78**, 10096 (2004).
5. A. T. Haase, *Nat. Rev. Immunol.* **5**, 783 (2005).
6. M. Pope, A. T. Haase, *Nat. Med.* **9**, 847 (2003).
7. M. R. Reynolds *et al.*, *J. Virol.* **79**, 9228 (2005).
8. Q. Li *et al.*, *Nature* **434**, 1148 (2005).
9. J. J. Mattapallil *et al.*, *Nature* **434**, 1093 (2005).
10. R. S. Veazey *et al.*, *Science* **280**, 427 (1998).
11. R. Ahmed, A. Salmi, L. D. Butler, J. M. Chiller, M. B. Oldstone, *J. Exp. Med.* **160**, 521 (1984).
12. E. J. Wherry, J. N. Blattman, K. Murali-Krishna, R. van der Most, R. Ahmed, *J. Virol.* **77**, 4911 (2003).
13. See supporting material on *Science* Online.
14. P. J. Skinner, M. A. Daniels, C. S. Schmidt, S. C. Jameson, A. T. Haase, *J. Immunol.* **165**, 613 (2000).
15. C. J. Miller *et al.*, *J. Virol.* **79**, 9217 (2005).
16. B. R. Mothe *et al.*, *J. Virol.* **76**, 875 (2002).
17. D. L. Barber *et al.*, *Nature* **439**, 682 (2006).
18. M. Matloubian, S. R. Kolhekar, T. Somasundaram, R. Ahmed, *J. Virol.* **67**, 7340 (1993).
19. M. Matloubian, T. Somasundaram, S. R. Kolhekar, R. Selvakumar, R. Ahmed, *J. Exp. Med.* **172**, 1043 (1990).
20. S. N. Mueller *et al.*, *Proc. Natl. Acad. Sci. U.S.A.* **104**, 15430 (2007).

21. We thank the Immunology Core Laboratory and Primate Services Unit of the California National Primate Research Center (CNPRC); D. Lu, T. Rourke, R. Dizon, and B. Vang for technical assistance; J. Sedgewick for assistance in setting up the confocal microscope to capture images of silver grains; D. Masopust for helpful discussion; and C. O'Neill and T. Leonard for help in preparing the manuscript and figures. Supported in part by NIH research grants AI48484 (A.T.H.), AI20048 (R.A.), and AI066314 (C.J.M.); National Center for Research Resources grant RR00169 (CNPRC, University of California, Davis); and a gift from the James B. Pendleton Charitable Trust (C.J.M.).

Supporting Online Material

www.sciencemag.org/cgi/content/full/323/5922/1726/DC1
Materials and Methods
Fig. S1
References

18 November 2008; accepted 9 February 2009
10.1126/science.1168676

Downloaded from www.sciencemag.org on March 27, 2009

Infection by Tubercular Mycobacteria Is Spread by Nonlytic Ejection from Their Amoeba Hosts

Monica Hagedorn,[1] Kyle H. Rohde,[2] David G. Russell,[2] Thierry Soldati[1]*

To generate efficient vaccines and cures for *Mycobacterium tuberculosis*, we need a far better understanding of its modes of infection, persistence, and spreading. Host cell entry and the establishment of a replication niche are well understood, but little is known about how tubercular mycobacteria exit host cells and disseminate the infection. Using the social amoeba *Dictyostelium* as a genetically tractable host for pathogenic mycobacteria, we discovered that *M. tuberculosis* and *M. marinum*, but not *M. avium*, are ejected from the cell through an actin-based structure, the ejectosome. This conserved nonlytic spreading mechanism requires a cytoskeleton regulator from the host and an intact mycobacterial ESX-1 secretion system. This insight offers new directions for research into the spreading of tubercular mycobacteria infections in mammalian cells.

Intracellular bacterial pathogens have evolved strategies to exploit host cell resources and replicate inside a variety of cell types, staying out of reach of the host's immune system. The concept is emerging that pathogenic bacteria evolved from environmental species by adapting to an intracellular lifestyle within free-living bacteria-eating protozoans. Consequently, cellular defense mechanisms that are active in animal immune phagocytes may have originated in amoebas (*1*, *2*). For example, during differentiation of the social amoeba *Dictyostelium* to form a multicellular structure, sentinel cells are deployed to combat pathogens (*1*).

Generally, infection follows the entry of a bacterium into a host cell, giving rise to a pathogen-containing vacuole usually called a phagosome. From this common starting point, pathogens subvert or resist the mechanisms that usually transform the phagosome into a bactericidal environment. Understanding of the passive or triggered uptake mechanisms and of the subsequent hijacking of host cell processes is increasing steadily, but little is known about how the pathogens exit their primary host cells and spread the infection.

Mycobacterium tuberculosis causes tuberculosis and other granulomatous lesions and is a major threat to human health. *M. marinum* is a close relative (*3*) responsible for fish and amphibian tuberculosis, in which it causes almost indistinguishable pathologies and lesions [reviewed in (*4*)]. Several elegant cross-species complementation studies between these two pathogens highlight their common mechanisms of pathogenicity [reviewed in (*4*)].

After passive uptake by immune phagocytes, *M. tuberculosis* and *M. marinum* arrest or bypass phago-lysosome maturation and replicate inside a compartment of endosomal nature (*5*–*7*).

[1]Département de Biochimie, Faculté des Sciences, Université de Genève, Sciences II, 30 quai Ernest Ansermet, CH-1211 Genève-4, Switzerland. [2]Department of Microbiology and Immunology, College of Veterinary Medicine, Cornell University, Ithaca, NY 14853, USA.

*To whom correspondence should be addressed. E-mail: thierry.soldati@unige.ch